

Lawrence Berkeley National Laboratory

LBL Publications

Title

Gas-Phase Complexes of Americium and Lanthanides with a Bis-triazinyl Pyridine: Reactivity and Bonding of Archetypes for F-Element Separations

Permalink

<https://escholarship.org/uc/item/2x726146>

Journal

The Journal of Physical Chemistry A, 124(15)

ISSN

1089-5639

Authors

Jian, Tian

Yu, Xiaojuan

Dan, David

et al.

Publication Date

2020-04-16

DOI

10.1021/acs.jpca.0c00675

Peer reviewed

Gas-Phase Complexes of Americium and Lanthanides with a Bis-Triazinyl Pyridine: Reactivity and Bonding of Archetypes for F-Element Separations

Tian Jian,¹ Xiaojuan Yu,² David Dan,³ Thomas E. Albrecht-Schmitt,³ Jochen Autschbach,^{2,*}
John K. Gibson^{1,*}

¹Chemical Sciences Division, Lawrence Berkeley National Laboratory, Berkeley, California
94720, USA

²Department of Chemistry, State University of New York at Buffalo, Buffalo, New York 14260,
USA

³Department of Chemistry and Biochemistry, Florida State University, 95 Chieftain Way,
Tallahassee, Florida 32306, USA

*Corresponding authors: jkgibson@lbl.gov; jochena@buffalo.edu

Abstract

Bis-triazinyl pyridines (BTPs) exhibit solution selectivity for trivalent americium over lanthanides (Ln), the origins of which remain uncertain. Here, electrospray ionization was used to generate gas-phase complexes $[ML_3]^{3+}$, where M=La, Lu, or Am, and L is the BTP 2,6-bis(5,6-diethyl-1,2,4-triazin-3-yl)-pyridine). Collision induced dissociation (CID) of $[ML_3]^{3+}$ in the presence of H₂O yielded protonated ligand $[L(H)]^+$, and hydroxide $[ML_2(OH)]^{2+}$ or hydrate $[ML(L-H)(H_2O)]^{2+}$ where (L-H)⁻ is a deprotonated ligand. Whereas solution affinities indicate stronger binding of BTPs towards Am³⁺ versus Ln³⁺, the observed CID process is contrastingly more facile for M = Am versus Ln. To understand the disparity, density functional theory was employed to compute potential energy surfaces for two possible CID processes, for M = La and Am. In accord with the CID results, both the rate determining transition state barrier and the net energy are lower for $[AmL_3]^{3+}$ versus $[LaL_3]^{3+}$, and for both product isomers, $[ML_2(OH)]^{2+}$ and $[ML(L-H)(H_2O)]^{2+}$. More facile removal of a ligand from $[AmL_3]^{3+}$ by CID does not necessarily contradict stronger Am³⁺-L binding as inferred from solution behavior. In particular, the formation of new bonds in the products can distort kinetics and thermodynamics expected for simple bond cleavage reactions. In addition to correctly predicting the seemingly anomalous CID behavior, the computational results indicate greater participation of Am 5f versus La 4f orbitals in metal-ligand bonding.

Introduction

Advanced actinide separation strategies reduce hazards and costs of managing radioactive wastes. As trivalent actinide (An) and lanthanide (Ln) metal ions have similar radii and chemical behavior, small bonding differences in An versus Ln coordination complexes are used to design separation ligands such as heterocyclic N-donors.¹⁻⁴ First synthesized in 1971,⁵ 2,6-bis(5,6-dialkyl-1,2,4-triazin-3-yl)-pyridines (BTPs) selectively extract Am^{3+} , as $[\text{Am}(\text{BTP})_3]^{3+}$, from Eu^{3+} .^{6, 7} Experiment and theory have illuminated the basis for actinide selectivity by BTPs. X-ray diffraction revealed trivalent uranium and lanthanide complexes $[\text{M}(\text{BTP})_3]^{3+}$ in solid state,⁸⁻¹⁰ with Ln-N bond lengths consistent with the lanthanide contraction but shortened U-N distances.⁹ Structures of BTP complexes with trivalent actinides (U, Pu, Am, and Cm) and lanthanides (Sm-Lu) in solution were established as $[\text{M}(\text{BTP})_3]^{3+}$ by extended X-ray absorption fine-structure, with unusually short Am-N distances.¹¹⁻¹⁴ Time-resolved laser-induced fluorescence and UV-Vis spectroscopy illuminated coordination chemistry, stability constants, and thermodynamics of $[\text{M}(\text{BTP})_3]^{3+}$ in solution, confirming a relationship between selectivity and metal-ligand bonding.^{11-13, 15-20} Evidence for enhanced covalence of Am-N versus Ln-N bonds in $[\text{M}(\text{BTP})_3]^{3+}$ was provided by ^{15}N NMR.²¹ Studies of gas-phase metal-BTP complexes have focused on trivalent lanthanides.²²⁻²⁴ Density functional theory (DFT) has provided insights into structures and bonding of $[\text{M}(\text{BTP})_3]^{3+}$ complexes,^{11, 13, 20, 25-34} but the origins of BTP selectivity remain unresolved.

A challenge for understanding the basis for efficacy of ligands for metal ion separations is that small differences in binding energies result in large separation factors. For example, an $\text{Am}^{3+}/\text{Ln}^{3+}$ separation factor of 3000 by a BTP ligand is considered remarkably good,³⁵ but even this feat corresponds to a difference in metal ion binding energies of only 4.8 kcal/mol at room temperature. Here, we employ a gas-phase approach to probe factors that might induce such selectivity. Electrospray ionization (ESI) of solutions of trivalent Am, La, or Lu with 2,6-bis(5,6-diethyl-1,2,4-triazin-3-yl)-pyridine (EtBTP = L) generated protonated ligand $[\text{L}(\text{H})]^+$ and complexes $[\text{ML}_3]^{3+}$ (M=Am, La, Lu), which were isolated in an ion trap for collision induced dissociation (CID). In apparent contrast to presumed stronger Am-L versus Ln-L bonding, $[\text{AmL}_3]^{3+}$ was more easily fragmented than both $[\text{LaL}_3]^{3+}$ and $[\text{LuL}_3]^{3+}$. However, the observed CID processes were not simple ligand L loss from $[\text{ML}_3]^{3+}$ to yield $[\text{ML}_2]^{3+}$, but rather reaction with water to yield $[\text{L}(\text{H})]^+$ and hydroxide $[\text{ML}_2(\text{OH})]^{2+}$ or hydrate $[\text{ML}(\text{L}-\text{H})(\text{H}_2\text{O})]^{2+}$. DFT calculations show that the observed CID processes are exothermic, with reaction energies and

transition state barriers lower for $M = \text{Am}$ versus $M = \text{La}$. Although more facile fragmentation of $[\text{AmL}_3]^{3+}$ appears to contradict the higher affinity of Am^{3+} for BTPs, consideration of the nature of the gas-phase phenomena informs otherwise.

Experimental methods

Caution! Radioactive Am-243 must be handled using special facilities and precautions.

The EtBTP ligand 2,6-bis(5,6-diethyl-1,2,4-triazin-3-yl)pyridine was synthesized by the two step procedure reported by Denecke and co-workers.²¹ The only variation from the reported synthesis was utilization of 3,4-hexanedione in the second step to incorporate the pendant ethyl groups.

The experiments were carried out using an Agilent 6340 quadrupole ion trap mass spectrometer (QIT/MS) with CID capabilities and a radiologically-contained ESI source described previously.³⁶ Cation complexes $[\text{L}(\text{H})]^+$ and $[\text{ML}_3]^{3+}$ ($M = \text{La}, \text{Lu}, \text{Am}$) were produced by ESI of ethanol solutions containing 0.1 mM MCl_3 or $\text{M}(\text{NO}_3)_3$ and 1 mM EtBTP (L). The employed Am-243 isotope undergoes alpha decay with a half-life of 7370 y. The complex ion of interest was isolated in the QIT and subjected to CID whereby energetic collisions with He to induce dissociation. The CID voltage is an instrumental parameter that indicates relative ion excitation. The He buffer gas pressure in the trap was $\sim 1 \times 10^{-4}$ torr, while that of background water was $\sim 1 \times 10^{-6}$ torr.³⁶ Positive ion mass spectra were acquired using the following parameters: solution flow rate, 60 $\mu\text{L}/\text{h}$; nebulizer gas pressure, 15 psi; capillary voltage offset and current, -3500 V and 4.883 nA; end plate voltage offset and current, -500 V and 125.000 nA; dry gas flow rate, 2 l/min; dry gas temperature, 325 °C; capillary exit, 150.1 V; skimmer, 40.0 V; octopole 1 and 2 DC, 12.00 V and 2.22 V; octopole RF amplitude, 200 Vpp; lens 1 and 2, -5.0 V and -60.0 V; trap drive, 77.9. The N_2 for nebulization and drying was from liquid boil-off. D_2O (Aldrich 99% D) or acetone- D_6 ($\text{C}_3\text{D}_6\text{O}$ 99.5% Aldrich) was introduced into the ion trap via a leak valve.³⁶ The pressure of D_2O relative to H_2O was determined by H/D exchange of $\text{UO}_2(\text{OH})^+$ and/or water-addition to UO_2^+ .³⁷

Computational methods

DFT calculations on gas-phase $[\text{LaL}_3]^{3+}$ and $[\text{AmL}_3]^{3+}$ were performed with the hybrid B3LYP exchange-correlation functional.³⁸⁻⁴⁰ Small-core Stuttgart energy-consistent relativistic pseudopotentials, ECP28MWB for La and ECP60MWB for Am, were used in conjunction with the available matching ANO type valence basis sets.^{41, 42} Computations using f-in-core

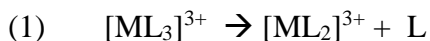
pseudopotentials ECP46MWB for La and ECP84MWB for Am assessed effects of not treating the La 4f and Am 5f electrons as part of the valence shell. Unless noted otherwise, computational results discussed in the text are those from the ‘f-in-valence’ (small core) pseudopotential calculations. The 6-31G(d) basis set was used for all light atoms (C, H, O, N).⁴³ Since the reactions involve proton transfer, we explored the effects from adding diffuse or polarization functions to the basis set of the relevant hydrogens. The energy differences in the mechanisms were the same to within 1 kcal/mol and therefore we proceeded with 6-31G(d,) in order to avoid an imbalanced basis. The high-spin septet spin states were calculated to be the lowest in energy for the Am³⁺ species. Spin contamination of the septet ground state was negligible. Vibrational frequency analysis was carried out at the same level of theory to determine the zero-point energy (ZPE) and characterize the stationary points. Minima and transition states were confirmed as such, with no or one imaginary frequency, respectively. All minima connected by a given transition state were confirmed by intrinsic reaction coordinate (IRC) computations.⁴⁴ Electronic and bonding properties of some key structures were studied using natural localized molecular orbital (NLMO) analysis. The calculations employed Gaussian 16 and the NBO 6.0 program.^{45, 46}

Results and Discussion

CID of EtBTP complexes

Protonated ligand [L(H)]⁺ was studied first. As shown in Figure 1, the dominant CID pathway is sequential loss of two fragments with mass 110, which corresponds to elimination of the moieties in red dashed lines. This CID fragmentation mirrors addition of hydrazine to pyridine carbonitrile used in BTP synthesis.⁵

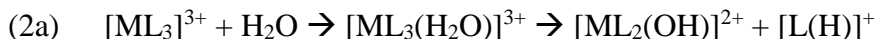
The central goal was to elucidate binding of BTP to trivalent An versus Ln. Lanthanides La³⁺ and Lu³⁺ have empty and filled 4f shells, respectively, and the largest and smallest ionic radii; An = Am has a partially filled 5f⁶ shell, and intermediate ionic radius⁴⁷—0.975 Å for Am³⁺, 1.032 Å for La³⁺, 0.861 Å for Lu³⁺. Colette et al.²³ reported CID of [Ln(iPrBTP)₃]³⁺ where iPrBTP is 2,6-bis(5,6-diisopropyl-1,2,4-triazin-3-yl)-pyridine) in which the four pendant ethyl groups in EtBTP are replaced by isopropyl groups. A dominant CID process there was elimination of neutral iPrBTP to yield [M(iPrBTP)₂]³⁺. We anticipated that CID of [M(EtBTP)₃]³⁺ would similarly proceed according to reaction (1), and furthermore that the CID efficiency would decrease as metal-ligand binding increased.



However, this is not what we found. ESI of solutions containing M^{3+} ($M = \text{La, Lu, or Am}$) and EtBTP (L) produced $[ML_3]^{3+}$. As shown in Figure 2, CID proceeded by charge-separation reaction (2) where the product complex may be hydroxide $[M(L)_2(OH)]^{2+}$ having two intact EtBTP, or hydrate $[M(L)(L-H)(H_2O)]^{2+}$ having an intact EtBTP and a deprotonated (EtBTP-H) $^-$. (In the notation used here, L-H indicates the subtraction of a proton from L.) In Figure 2, anticipated ligand loss reaction (1) is not apparent, possibly reflecting different conditions than used for CID of the iPrBTP complexes.²³ Also not observed is the cleavage evident in Figure 1 for the protonated ligand. Notably, CID of $[AmL_3]^{3+}$ in Figure 2 is more efficient—i.e., more dissociation—than that of $[LaL_3]^{3+}$ or $[LuL_3]^{3+}$. However, the present computations show that this is *not* indicative of weaker Am-L binding.



The reactant and product cations in reaction (2) are identified in the mass spectra in Figure 2, while inferred neutral H_2O is a background gas in the ion trap.³⁷ As metal-ligand binding in $[ML_3]^{3+}$ was expected to parallel the higher solution affinity of BTPs towards Am^{3+} versus Ln^{3+} ,⁶ reaction (1) was expected to be lower energy and more efficient for $M = Ln$ versus $M = Am$, the opposite of what was found for CID reaction (2). The unanticipated CID results shifted the focus from simple ligand removal reaction (1) to observed reaction (2). We consider two essential scenarios as revealing key aspects of reaction (2): the eliminated proton comes from water to yield $[ML_2(OH)]^{2+}$, reaction (2a); or the proton comes from a ligand to yield $[ML(L-H)(H_2O)]^{2+}$, reaction (2b). Ligand substitution reactions to differentiate between the two product isomers suggested some hydrate product as in (2b), but were overall inconclusive (see SI). It should be noted that a deprotonated coordinating ligand such as in reaction (2b) was separately found in CID of $[ML_3(NO_3)]^{2+}$ to yield $[ML_2(L-H)]^{2+}$ and HNO_3 (SI Figure S7). An alternative to reaction (2b) is elimination of a deprotonated ligand to yield $[ML(L-H)]^{2+}$, which then adds water. However, our DFT calculations indicate that the water in $[ML_3(H_2O)]^{3+}$ is not directly involved in the mechanism for reaction (2b) such that this process provides essential insights into intra-ligand proton transfer and is thus appropriate for the present assessment.



To further probe the CID process, D_2O was introduced into the ion trap at a pressure comparable to that of H_2O . If the proton comes from water as in reaction (2a) then CID with D_2O

should yield $[L(D)]^+$. The actual result in Figure 3 is dominant $[L(H)]^+$ in the presence of D_2O , with the minor $[L(D)]^+$ attributed to isotope-exchange between $[L(H)]^+$ and D_2O (see SI). The absence of appreciable $[L(D)]^+$ is consistent with intra-ligand proton transfer as in reaction (2b).

Reaction potential energy surfaces

Although the experiments point to reaction (2b), both (2a) and (2b) were computationally assessed with a focus on understanding more facile CID for $M = Am$ versus $M = La$. Computed structures of alternative hydroxide $[ML_2(OH)]^{2+}$ and hydrate $[ML(L-H)(H_2O)]^{2+}$ are shown in Figure 4. The hydroxide structure has two tridentate coordinating ligands and a hydroxyl group. In the more peculiar hydrate structure, there is a tridentate ligand, a hydrating water, and an EtBTP ligand that has been deprotonated at an α -C site in a pendant CH_2CH_3 group. The distance between the metal center and the carbanion site in $[:CHCH_3]$ —5.27 Å for $M = La$ and 5.63 Å for $M = Am$ —is too long for direct bonding such that these $[ML(L-H)(H_2O)]^{2+}$ are formally zwitterions. The hydroxide structures were found to be lower energy than the hydrates, by 26.2 kcal/mol for $M = La$ and by 23.2 kcal/mol for $M = Am$. It should be emphasized that these particular hydrate structures may not be the global minima but are appropriate for the present assessment.

The computed potential energy surfaces (PESs) for reaction (2a) are shown in Figure 5, with the energies of the various species given in Table 1. Energies are provided for pseudopotentials with the Ln 4f or Am 5f orbitals treated as both in the core, and in the valence shell. The structures of the species on the PES are in Figures 6 and 7, with selected interatomic distances in Table 2. Reaction (2a) proceeds through the following steps on the PES in Figure 5, where separated reactants $[ML_3]^{3+}$ and H_2O define zero energy ($\Delta E \equiv 0$). (1) The reaction commences via the formation of a weakly bound pre-reactive complex **RC**, at only ca. 5-6 kcal/mol below the reactants. The M-O distance in **RC** is large (5.0 Å), and the water is attached by a hydrogen bond to a ligand N atom in an outer-sphere coordination arrangement. (2) The reaction proceeds to a first transition state **TS1** in which the water reorients to yield intermediate **IM** at ca. 6-8 kcal/mol below the reactants, where the M-O distances in **IM** are around 2.6 Å. The M-O distance in **TS1**, ca. 3.7-4.0 Å, is still too large for a significant bonding interaction such that the dominant interaction remains H-bonds to ligand N atoms, with the water remaining outer-sphere coordination. (3) In second transition state **TS2** a proton is transferred from H_2O to a pyridyl N atom, to ultimately yield separated products (**Prod**) $[ML_2(OH)]^{2+}$ and $[L(H)]^+$. The energy released in the final step is substantial, with overall reaction (2a) exothermic by -47.9 kcal/mol for

M = La and -51.1 kcal/mol for M = Am, and largely driven by strong ionic bonding interactions in $[\text{ML}_2(\text{OH})]^{2+}$.

The computed PESs for reaction (2a) predict that water should spontaneously associate with $[\text{ML}_3]^{3+}$ to yield hydrates **RC**. However, isolating the $[\text{ML}_3]^{3+}$ complexes in the presence of background water for the longest possible reaction time of 10 s did not yield detectable hydrates or other products (see SI Figure S6). As discussed elsewhere,³⁷ weakly bound outer-sphere hydrates such as **RC** are not observed under these conditions. For example, addition of H_2O to UO_2^+ is exothermic by -32 kcal/mol and the resulting strongly bound inner-sphere hydrate $[\text{UO}_2(\text{H}_2\text{O})]^+$ is apparent under the present experimental conditions after only 0.05 s (Figure S5). In contrast, addition of H_2O to $[\text{UO}_2(\text{H}_2\text{O})_4]^+$ is exothermic by -11 kcal/mol but this process is not detected after 5 s reaction.³⁷ As the water molecule is bound by <10 kcal/mol for both **RC** and **IM** on the PESs in Figure 4, these species are similarly not expected to be observed. Net reaction (2a) is substantially more exothermic than simple hydration, but this hydrolysis is not observed in the absence of CID excitation, consistent with computed **TS2** barriers of >4 kcal/mol.

For separated reactants **R**, **RC**, **TS1** and **IM**, the PES for reaction (2b) is identical to that in Figure 5 for (2a). However, instead of proton-transfer from water via **TS2**, the proton is transferred from a ligand via **TS3** in Figure 5 with the structure shown in Figure 8. **TS3** then yields the hydrate shown in Figure 4 and protonated ligand $[\text{L}(\text{H})]^+$. The PES in Figure 5 and energies in Table 1 show that **TS3** are more than 30 kcal/mol higher than **TS2**, and the hydrate products are more than 23 kcal/mol less stable than the hydroxides. The possibility of proton transfer in the hydrates $[\text{ML}(\text{L}-\text{H})(\text{H}_2\text{O})]^{2+}$ to yield lower-energy hydroxides $[\text{ML}_2(\text{OH})]^{2+}$ was not assessed because the kinetic differences for M = La versus M = Am are captured by **TS3** regardless of potential subsequent rearrangement of the product to a lower energy structure.

Although **TS3** is much higher than **TS2**, for both reactions (2a) and (2b) the barrier is lower for M = Am versus M = La. Thus, both mechanisms are consistent with the observation of more facile CID for M = Am versus M = La. The overall reaction energies exhibit a similar relationship, with the products lower energy for M = Am versus M = La for both the hydroxide and hydrate structures. The accord between the computational and experimental results, and the parallel between the rate-determining transition states and net reaction energies, prompts attention to the following: If the BTP ligand is more strongly bound to Am^{3+} versus La^{3+} , why are ligand elimination reactions (2a) and (2b) more exothermic and facile for M = Am?

Factors affecting PES energies

For **RC**, **TS1** and **IM** the computed energies in Table 1 are similar, to within 2 kcal/mol, for f-in-core versus f-in-valence basis sets, and also similar for M = La versus M = Am. For **RC** and **TS1** this similarity reflects that the metal center does not directly interact with the hydrogen-bonded water. However, in **IM** the M-O distance of ca. 2.6 Å is sufficiently short for significant interaction, but such electrostatic hydrate bonding should not vary significantly for different Ln³⁺ and An³⁺.⁴⁸ The reactions become more differentiated at **TS2** in which a proton is transferred from water to the N_P (P = pyridyl) of the leaving ligand (N_{leave}). In **TS2** two of the three coordinating N_{leave} have been separated from the metal center, with M-N_{leave} distances of >4 Å. The third M-N_{leave} distance is shorter in **TS2** than in **IM** such that immediately before ligand elimination this bond shortens. The energy differences for **TS2** and **Prod** [ML₂(OH)]²⁺ between f-in-core versus f-in-valence, and between M = La and M = Am, reflect the strengths of the disrupted M-N_{leave} and created M-O_{OH} bonds. Inclusion of f orbitals in the valence shell lowers the energies of both **TS2** and **Prod** [ML₂(OH)]²⁺, with the larger energy change for M = Am indicating greater bonding involvement of Am 5f versus La 4f.

The persisting conundrum is that **TS2** and **Prod** [ML₂(OH)]²⁺ for reaction (2a) are lower in energy for M = Am versus M = La, despite supposedly stronger metal-ligand binding in [AmL₃]³⁺ versus [LaL₃]³⁺. Transformation of [ML₃(H₂O)]³⁺ to [ML₂(OH)]²⁺ and [L(H)]⁺ does not simply involve removal of an intact ligand, but also formation of a strong M-O_{OH} bond, with the net transformation more energetically favorable for M = Am versus M = La. It is thus not contradictory that such bond cleavage/formation does not necessarily reflect only the relative strengths of the cleaved bonds.

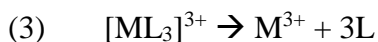
As for reaction (2a), the energies for reaction (2b) **TS3** and **Prod** [ML(L-H)(H₂O)]²⁺ are lower for M = Am versus M = La, though instead of a strong M-O_{OH} bond there is a weaker dative M³⁺-(H₂O) bond that should be similar for different M.⁴⁸ A peculiar feature of the [ML(L-H)(H₂O)]²⁺ species is the (L-H)⁻ moiety. As shown in Figure 4, the deprotonated carbanion site in (L-H)⁻ is too far from the metal center for direct bonding. Metal-nitrogen distances for the [ML₃]³⁺ complexes and products [ML(L-H)(H₂O)]²⁺ are in Table 2, along with the difference, Δ[La-Am]. For ion-dipole bonds, Δ[La-Am] should be ~0.057 Å, which is simply the difference between the ionic radii of La³⁺ (1.032 Å) and Am³⁺ (0.975 Å).⁴⁷ The larger difference of 0.105 Å for M-N_P in [ML₃]³⁺ is consistent with enhanced Am-N covalent bonding. The M-N distances for the intact

ligand in $[\text{ML}(\text{L-H})(\text{H}_2\text{O})]^{2+}$ are similar to those in $[\text{ML}_3]^{3+}$, with the M-N_T ($\text{T} = \text{triazyl}$) slightly (by $<0.07 \text{ \AA}$) shortened and the M-N_P slightly elongated. For deprotonated $(\text{L-H})^-$, relative to $[\text{ML}_3]^{3+}$ the M-N distances are moderately shortened for N_P and the N_T far from the deprotonation site. The M-N_T distances for the N_T that is close to the deprotonation site in $(\text{L-H})^-$ are substantially more shortened relative to the corresponding distances in $[\text{ML}_3]^{3+}$. For $\text{M} = \text{Am}$, this M-N_T distance is shortened by 0.138 \AA , to a distance of 2.507 \AA ; for $\text{M} = \text{La}$ it is more drastically shortened, by 0.341 \AA to a distance of 2.368 \AA . Whereas the other M-N distances are comparable to those in other coordination complexes,⁴⁹ this Am-N_T distance, and more so this La-N_T distance, indicate a strong bond such as in metal nitrido complexes.⁵⁰ These short M-N_T bonds indicate that the $[\text{ML}(\text{L-H})(\text{H}_2\text{O})]^{2+}$ complexes are not simple zwitterions with an isolated carbene site on an ethyl group. Rather there is evidently some charge transfer to a N_T site, which results in stronger binding to the metal center. The quite different bond distances to this N_T for $\text{M} = \text{La}$ and $\text{M} = \text{Am}$ suggest different charge distributions and binding. As with the hydroxide products, differing binding of metals to $(\text{L-H})^-$ in these products need to be considered in assessing the reaction energies, and the related transition state barriers.

From the results in Table 1 it is apparent that the **TS2** and **Prod** energy reductions upon inclusion of f orbitals in the valence shell are generally greater for $\text{Am } 5f$ versus $\text{La } 4f$, suggesting more involvement of $5f$ orbitals in bonding. NLMO analysis results in Table 3 specifically for the M-O bonds in **TS2** substantiate this conclusion. Both the La-O and Am-O bonds are found to be dominated by oxygen-based orbitals, 94% and 92%, respectively, which is indicative of partially covalent oxygen-to-metal donation bonding. For the metal-based orbital participation the contributions include 16% $\text{La } 4f$ and 49% $\text{Am } 5f$. The net result is M-O bond contributions that are only 1% $\text{La } 4f$ and 4% $\text{Am } 5f$. Although both $\text{La } 4f$ and $\text{Am } 5f$ orbitals are comparatively minor participants in these metal-oxo bonds, the $\text{Am } 5f$ involvement is critical for explaining why the CID fragmentation is more facile for Am than La : When the calculations are carried out with the f -in-core pseudopotentials, there is virtually no difference between the reaction profiles for Am versus La .

A particularly appealing process for assessing ligand binding to metal cations is dissociation reaction (3). Preliminary calculations (not shown) for reaction (3) at the DFT level suggested stronger BTP binding energies and increased metal-ligand bond orders with Am^{3+} versus La^{3+} , a result in accord with relative binding affinities in solution. We leave a detailed report

on these energies for a subsequent publication as the contributions from the spin-orbit coupling to the energy of reaction (3) are most likely not negligible and require computations that go beyond the scope of this work.



Conclusions

CID of gas-phase $[\text{ML}_3]^{3+}$ complexes, where L is an EtBTP, in the presence of H_2O yielded protonated ligand $[\text{L}(\text{H})]^+$ and either hydroxide $[\text{ML}_2(\text{OH})]^{2+}$ or hydrate $[\text{ML}(\text{L}-\text{H})(\text{H}_2\text{O})]^{2+}$ ($\text{M} = \text{La}, \text{Lu}, \text{Am}$). In seeming contradiction to stronger binding of BTPs to Am^{3+} in solution, CID fragmentation was more facile for $[\text{AmL}_3]^{3+}$ versus $[\text{LaL}_3]^{3+}$ and $[\text{LuL}_3]^{3+}$. PESs computed for pathways to both the hydroxide and hydrate for $\text{M} = \text{La}$ and $\text{M} = \text{Am}$ predict lower energies for the transition state and products for $\text{M} = \text{Am}$, which is consistent with the CID results. The DFT computations also revealed a greater influence of Am 5f versus La 4f orbitals on reaction energies, indicating greater participation of the 5f orbitals in bonding.

Consideration of bonds cleaved and formed in the CID processes indicate that those formed could dominate differences in reaction energies, such that more weakly bound ligands are not necessarily eliminated more easily. Simple ligand elimination from $[\text{ML}_3]^{3+}$ to yield $[\text{ML}_2]^{3+}$ and neutral L was not observed; as the energy for this process is the binding difference for three versus two ligands, it would not necessarily track the net metal-ligand binding in $[\text{ML}_3]^{3+}$. Instead, direct evaluation of metal-ligand bond strengths in $[\text{ML}_3]^{3+}$ would require complete dissociation to yield M^{3+} and three L (reaction 3), a process that is experimentally inaccessible due to the reactive nature of metal trications.⁵¹

Although simple gas-phase reactions of coordination complexes such as reported here do not necessarily directly reveal metal-ligand binding energies, they do reveal essential aspects of bonding and reactivity, including differences relevant to real-world processes such as separations. In the present work, DFT correctly predicted a seemingly anomalous observation, and furthermore provided insights into the origins of this apparent discrepancy.

Acknowledgements

This work was fully supported by the Center for Actinide Science and Technology, an Energy Frontier Research Center funded by the U.S. Department of Energy, Office of Science, Basic Energy Sciences under Award Number DE-SC0016568.

Supporting Information

CID mass spectra of $[\text{ML}_3]^{3+}$, $[\text{ML}_3(\text{NO}_2)]^{2+}$, and $[\text{ML}_3]^{3+}$ in $\text{H}_2\text{O}/\text{D}_2\text{O}$; results for reactions of $[\text{ML}_2(\text{OH})]^{2+}$ with acetone, and $[\text{L}(\text{H})]^+$ with D_2O , UO_2^+ with $\text{H}_2\text{O}/\text{D}_2\text{O}$, and $[\text{ML}_3]^{3+}$ with H_2O . Gibbs free energies, enthalpies and internal energies at 298 K for species in reaction (2).

Table 1. Energies (kcal/mol) for species on the reaction (2) PES in Figure 5 for $\text{M} = \text{La}$ and $\text{M} = \text{Am}$ using basis sets with 4f / 5f in-core or in-valence.^a

	RC	TS1	IM	TS2	Prod $[\text{ML}_2(\text{OH})]^{2+}$ + HL^+	TS3 ^b	Prod ^b $[\text{ML}(\text{L}-\text{H})(\text{H}_2\text{O})]^{2+}$ + HL^+
La / 4f core	-5.1	-2.9	-6.0	10.8	-41.9		
La / 4f valence	-4.9	-2.7	-8.0	8.5	-47.9	40.9	-21.7
$\Delta[\text{La core} \rightarrow \text{valence}]$	+0.2	+0.2	-2.0	-2.3	-6.0		
Am / 5f core	-5.1	-1.9	-6.0	9.7	-42.4		
Am / 5f valence	-5.8	-2.5	-6.2	4.1	-51.1	39.0	-27.9
$\Delta[\text{Am core} \rightarrow \text{valence}]$	-0.7	-0.6	-0.2	-5.6	-8.7		

^a Energies are relative to reactants at 0 K, including zero-point vibrational energies. Δ is the change in energy upon changing the effective core potentials from including the 4f/5f orbitals to a treatment of these orbitals in the valence space.

^b Energies for alternative **TS3** in Figure 8 that results in hydrate $[\text{ML}(\text{L}-\text{H})(\text{H}_2\text{O})]^+$ in Figure 4.

Table 2. Selected M-N distances (Å) for $[ML_3]^{3+}$ and $[ML(L-H)(H_2O)]^{2+}$.^a

	M = La	M = Am	$\Delta[La-Am]^b$
$N1_T$ & $N3_T$	2.709	2.645	0.064
$N2_P$	2.732	2.627	0.105
Na_T	2.642	2.615	0.027
Nb_P	2.777	2.706	0.071
Nc_T	2.755	2.715	0.040
Nd_T	2.583	2.533	0.050
Ne_P	2.660	2.580	0.080
Nf_T	2.368	2.507	-0.139

^a B3LYP/ECP28MWB_ANO(La):ECP60MWB_ANO():6-31G(d)(C,H,N,O) level of theory with N atoms identified in Figures 4 and 7. N_T denotes a triazolyl N atom, and N_P a pyridyl N atom

^b Difference between distances for M = La and M = Am; the reference difference between the ionic radii of La^{3+} (1.032 Å) and Am^{3+} (0.975 Å) is 0.057 Å.⁴⁷

Table 3. Natural localized molecular orbital (NLMO) analysis of La-O and Am-O σ bonds in TS2 at B3LYP/ECP28MWB_ANO(La):ECP60MWB_ANO(Am):6-31G(d)(C,H,N,O) level of theory.

	M = La	M = Am
oxygen	94% (46% 2s, 54% 2p)	92% (7% 2s, 93% 2p)
metal	6% (16% 6s, 68% 5d, 16% 4f)	8% (7% 7s, 1% 7p, 43% 6d, 49% 5f)

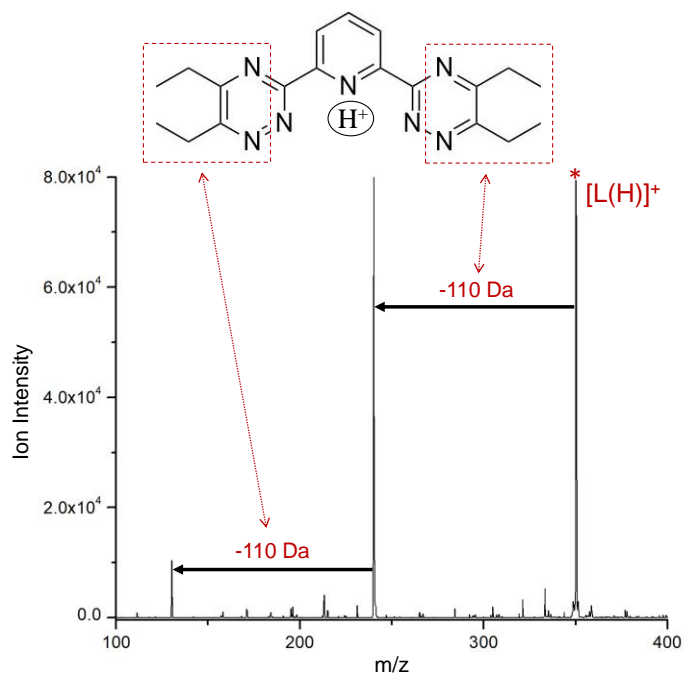


Figure 1. CID mass spectrum of $[L(H)]^+$ (nominal 0.65 V CID). The dashed lines on the structure of $[L(H)]^+$ shown at the top identify fragments corresponding to the observed loss of $m/z = 110$.

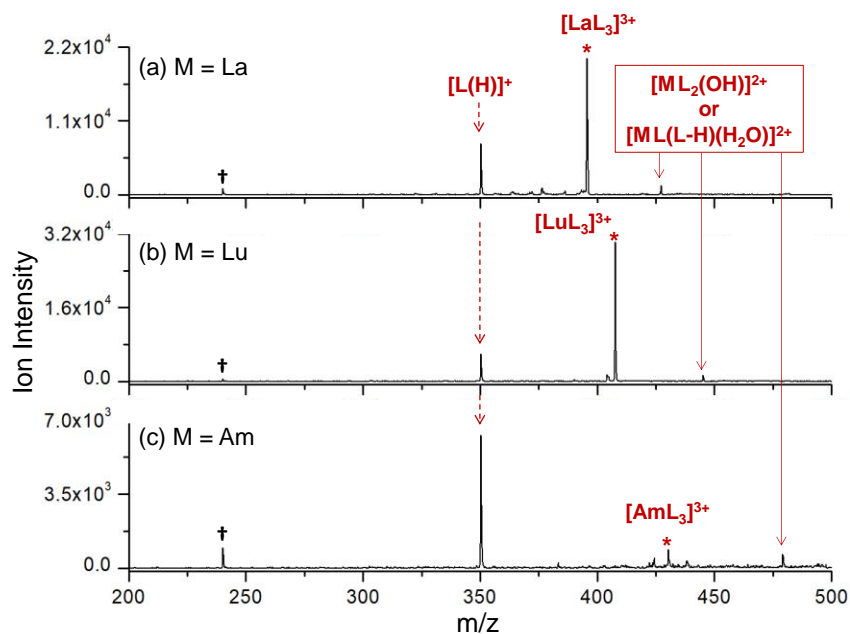


Figure 2. CID mass spectra of $[ML_3]^{3+}$ (identified by *) for (a) M = La, (b) M = Lu, and (c) M = Am (nominal 0.55 V CID). The only observed products are $[L(H)]^+$, and $[ML_2(OH)]^{2+}$ or $[ML(L-H)(H_2O)]^{2+}$. CID is most efficient for M = Am. The features at 240 m/z indicated by a dagger (†) correspond to secondary loss of 110 Da from $[L(H)]^+$, which is the primary process in Figure 1.

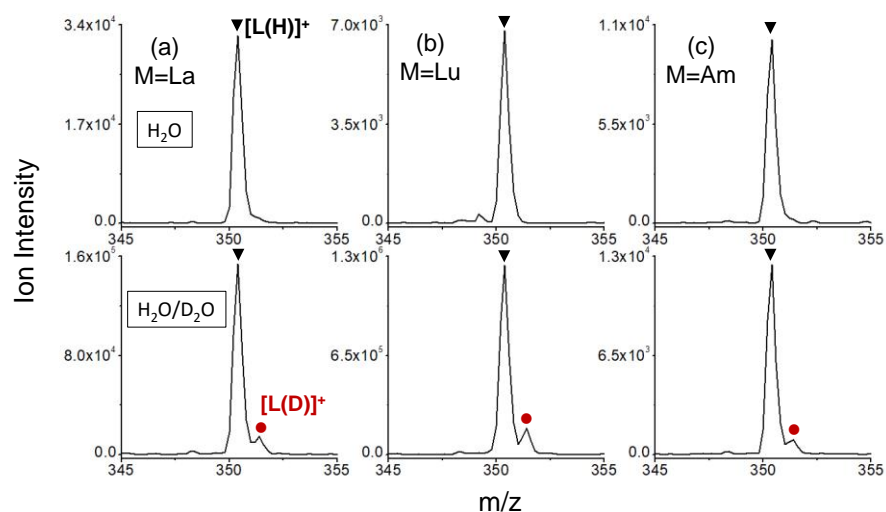


Figure 3. Portion of CID mass spectra of $[ML_3]^{3+}$ showing the protonated ligand product for (a) $M = La$, (b) $M = Lu$, and (c) $M = Am$ (nominal 0.45 V CID). Upper spectra in normal background H_2O yield only $[L(H)]^+$ (\blacktriangledown). Lower spectra with D_2O at about the same pressure as H_2O yield very minor $[L(D)]^+$ (\bullet), which indicates that the proton is from a ligand rather than water.

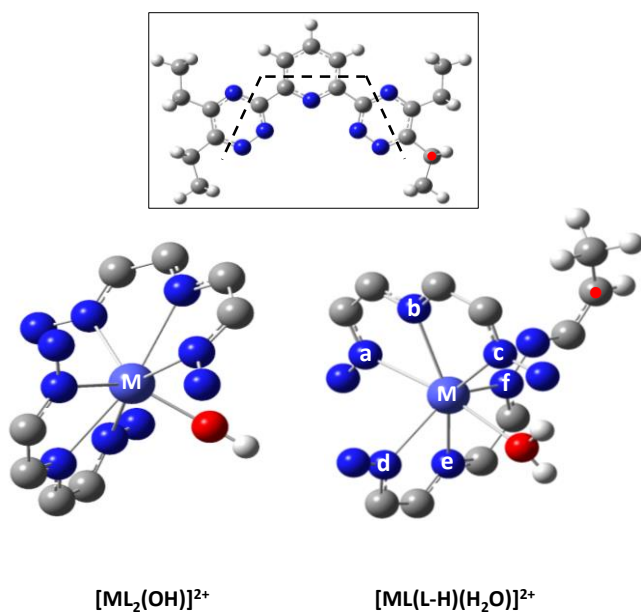


Figure 4. Computed structures of hydroxide $[ML_2(OH)]^{2+}$ and hydrate $[ML(L-H)(H_2O)]^{2+}$ using f -in-valence basis sets ECP28MWB for $M = La$ and ECP60MWB for $M = Am$. Central blue atom = M ; red = O ; dark blue = N . Ligands are truncated for clarity (inset). Deprotonation in $(L-H)^-$ is at the α -C in a CH_2CH_3 group (red dot). Hydroxides are lower in energy than hydrates, by 26.2 and 23.2 kcal/mol for $M = La$ and Am , respectively. $M-N$ distances for labeled N are in Table 2.

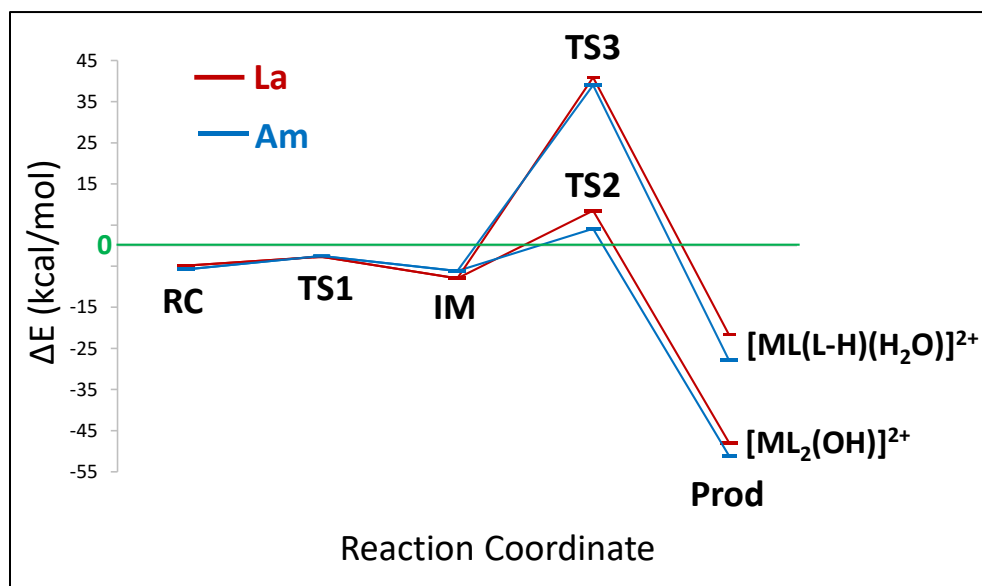


Figure 5. Computed PES for reactions (2a) via **TS2** and (2b) via **TS3** for $M = \text{La}$ (red) and $M = \text{Am}$ (blue). Separated reactants $\mathbf{R}-\text{H}_2\text{O}$ and $[\text{ML}_3]^{3+}$ —define zero energy. **Prod** designates products $[\text{L}(\text{H})]^+$ and either $[\text{ML}_2(\text{OH})]^{2+}$ from **TS2** or $[\text{ML}(\text{L}-\text{H})(\text{H}_2\text{O})]^{2+}$ from **TS3**. Energies are for basis sets with La 4f or Am 5f in the valence shell.

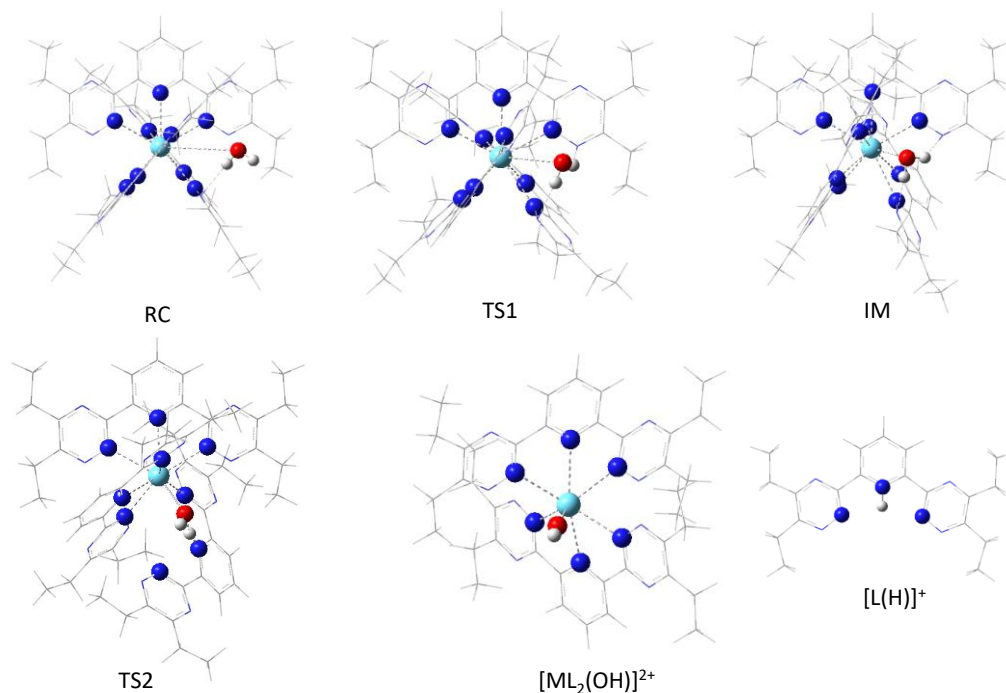


Figure 6. Computed structures of species on the PES for reaction (2a) in Figure 5. **RC** = reactant complex $[\text{ML}_3 \cdot (\text{H}_2\text{O})]^{3+}$; **TS1** = first transition state; **IM** = intermediate complex; **TS2** = second transition state. Light blue = La or Am; red = O; dark blue = N.

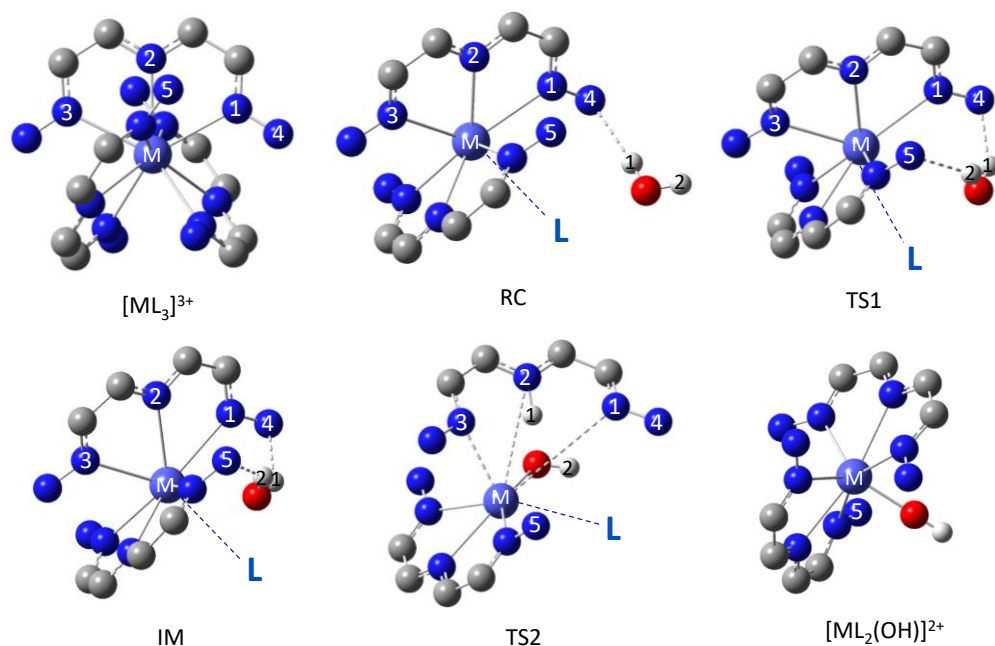


Figure 7. The same structures as in Figure 6 but with the ligands truncated as in Figure 4. For further clarity, in some structures one ligand is omitted, as indicated by L. Metal-atom distances in Table 2 and Figure 8 correspond to atoms O (red) and the numbered N (blue).

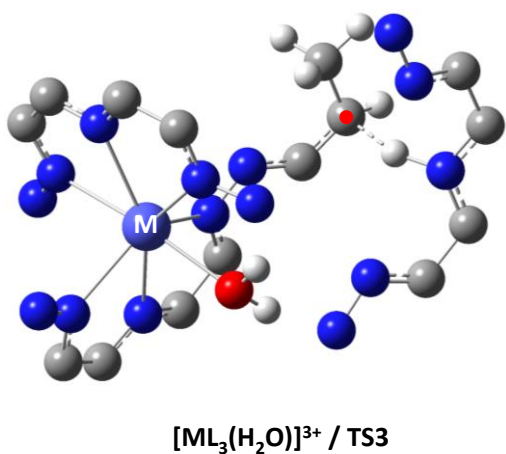


Figure 8. Structure of the **TS3** for reaction (2b) on the upper PES in Figure 5 that yields products $[L(H)]^+$ and $[ML(L-H)(H_2O)]^{2+}$ (structure in Figure 4). Proton transfer to the departing ligand is from the C atom with a red dot.

References

1. Kolarik, Z., Complexation and separation of lanthanides(III) and actinides(III) by heterocyclic N-donors in solutions. *Chem. Rev.* **2008**, *108* (10), 4208-4252.
2. Ekberg, C.; Fermvik, A.; Retegan, T.; Skarnemark, G.; Foreman, M. R. S.; Hudson, M. J.; Englund, S.; Nilsson, M., An overview and historical look back at the solvent extraction using nitrogen donor ligands to extract and separate An(III) from Ln(III). *Radiochimica Acta* **2009**, *96* (4-5), 225-233.
3. Lewis, F. W.; Hudson, M. J.; Harwood, L. M., Development of highly selective ligands for separations of actinides from lanthanides in the nuclear fuel cycle. *Synlett* **2011**, *2011* (18), 2609-2632.
4. Panak, P. J.; Geist, A., Complexation and extraction of trivalent actinides and lanthanides by triazinylpyridine N-donor ligands. *Chem. Rev.* **2013**, *113* (2), 1199-1236.
5. Case, F. H., The preparation of 2,4- and 2,6-bis-triazinyl and triazolanyl derivatives of pyridine. *Journal of Heterocyclic Chemistry* **1971**, *8* (6), 1043-1046.
6. Kolarik, Z.; Müllich, U.; Gassner, F., Selective extraction of Am(III) over Eu(III) by 2,6-dotriazolyl- and 2,6-ditriazinylpyridines. *Solvent Extraction and Ion Exchange* **1999**, *17* (1), 23-32.
7. Kolarik, Z.; Mullich, U.; Gassner, F., Extraction of Am(III) and Eu(III) nitrates by 2-6-di-(5,6-dipropyl-1,2,4-triazin-3-yl)pyridines 1. *Solvent Extraction and Ion Exchange* **1999**, *17* (5), 1155-1170.
8. Drew, M. G. B.; Guillaneux, D.; Hudson, M. J.; Iveson, P. B.; Russell, M. L.; Madic, C., Lanthanide(III) complexes of a highly efficient actinide(III) extracting agent – 2,6-bis(5,6-dipropyl-1,2,4-triazin-3-yl)pyridine. *Inorganic Chemistry Communications* **2001**, *4* (1), 12-15.
9. B. Iveson, P.; Rivière, C.; Guillaneux, D.; Nierlich, M.; Thuéry, P.; Ephritikhine, M.; Madic, C., Selective complexation of uranium(III) over cerium(III) by 2,6-bis(5,6-dialkyl-1,2,4-triazin-3-yl)pyridines: 1H NMR and X-ray crystallography studies. *Chemical Communications* **2001**, *0* (16), 1512-1513.
10. Berthet, J.-C.; Miquel, Y.; Iveson, P. B.; Nierlich, M.; Thuéry, P.; Madic, C.; Ephritikhine, M., The affinity and selectivity of terdentate nitrogen ligands towards trivalent lanthanide and uranium ions viewed from the crystal structures of the 1 : 3 complexes. *J. Chem. Soc., Dalton Trans.* **2002**, (16), 3265-3272.
11. Denecke, M. A.; Rossberg, A.; Panak, P. J.; Weigl, M.; Schimmelpfennig, B.; Geist, A., Characterization and comparison of Cm(III) and Eu(III) complexed with 2,6-di(5,6-dipropyl-1,2,4-triazin-3-yl)pyridine using EXAFS, TRFLS, and quantum-chemical methods. *Inorg. Chem.* **2005**, *44* (23), 8418-8425.
12. Denecke, M. A.; Panak, P. J.; Burdet, F.; Weigl, M.; Geist, A.; Klenze, R.; Mazzanti, M.; Gompfer, K., A comparative spectroscopic study of U(III)/Am(III) and Ln(III) complexed with N-donor ligands. *Comptes Rendus Chimie* **2007**, *10* (10), 872-882.
13. Banik, N. L.; Schimmelpfennig, B.; Marquardt, C. M.; Brendebach, B.; Geist, A.; Denecke, M. A., Characterization of redox sensitive plutonium(III) complexed with alkylated 2,6-ditriazinylpyridine (BTP) in organic solution. *Dalton Transactions* **2010**, *39* (21), 5117-5122.
14. Banik, N. L.; Denecke, M. A.; Geist, A.; Modolo, G.; Panak, P. J.; Rothe, J., 2,6-Bis(5,6-dipropyl-1,2,4-triazin-3-yl)-pyridine: Structures of An(III) and Ln(III) 1:3 complexes and selectivity. *Inorganic Chemistry Communications* **2013**, *29*, 172-174.
15. Colette, S.; Amekraz, B.; Madic, C.; Berthon, L.; Cote, G.; Moulin, C., Europium(III) interaction with a polyaza-aromatic extractant studied by time-resolved laser-induced luminescence: A thermodynamical approach. *Inorg. Chem.* **2004**, *43* (21), 6745-6751.
16. Miguirditchian, M.; Guillaneux, D.; François, N.; Airvault, S.; Ducros, S.; Thauvin, D.; Madic, C.; Illemassène, M.; Lagarde, G.; Krupa, J. C., Complexation of lanthanide(III) and actinide(III) cations with tridentate nitrogen-donor ligands: A luminescence and spectrophotometric study. *Nuclear Science and Engineering* **2006**, *153* (3), 223-232.

17. Hubscher-Bruder, V.; Haddaoui, J.; Bouhroum, S.; Arnaud-Neu, F., Recognition of some lanthanides, actinides, and transition- and heavy-metal cations by N-donor ligands: Thermodynamic and kinetic aspects. *Inorg. Chem.* **2010**, *49* (4), 1363-1371.
18. Trumm, S.; Panak, P. J.; Geist, A.; Fanghänel, T., A TRLFS study on the complexation of Cm(III) and Eu(III) with 2,6-bis(5,6-dipropyl-1,2,4-triazin-3-yl)pyridine in water/methanol mixture. *European Journal of Inorganic Chemistry* **2010**, *2010* (19), 3022-3028.
19. Rawat, N.; Bhattacharyya, A.; Ghosh, S. K.; Gadly, T.; Tomar, B. S., Thermodynamics of complexation of lanthanides with 2,6-bis(5,6-diethyl-1,2,4-triazin-3-yl) pyridine. *Radiochimica Acta* **2011**, *99* (11), 705-712.
20. Bhattacharyya, A.; Kim, E.; Weck, P. F.; Forster, P. M.; Czerwinski, K. R., Trivalent actinide and lanthanide complexation of 5,6-dialkyl-2,6-bis(1,2,4-triazin-3-yl)pyridine (RBTP; R = H, Me, Et) derivatives: A combined experimental and first-principles study. *Inorg. Chem.* **2013**, *52* (2), 761-776.
21. Adam, C.; Kaden, P.; B. Beele, B.; Müllich, U.; Trumm, S.; Geist, A.; J. Panak, P.; A. Denecke, M., Evidence for covalence in a N-donor complex of americium(III). *Dalton Transactions* **2013**, *42* (39), 14068-14074.
22. Colette, S.; Amekraz, B.; Madic, C.; Berthon, L.; Cote, G.; Moulin, C., Use of electrospray mass spectrometry (ESI-MS) for the study of europium(III) complexation with bis(dialkyltriazinyl)pyridines and its implications in the design of new extracting agents. *Inorg. Chem.* **2002**, *41* (26), 7031-7041.
23. Colette, S.; Amekraz, B.; Madic, C.; Berthon, L.; Cote, G.; Moulin, C., Trivalent lanthanide interactions with a terdentate bis(dialkyltriazinyl)pyridine ligand studied by electrospray ionization mass spectrometry. *Inorg. Chem.* **2003**, *42* (7), 2215-2226.
24. Steppert, M.; Walther, C.; Geist, A.; Fanghänel, T., Direct nano ESI time-of-flight mass spectrometric investigations on lanthanide BTP complexes in the extraction-relevant diluent 1-octanol. *New J. Chem.* **2009**, *33* (12), 2437-2442.
25. Ionova, G.; Rabbe, C.; Guillaumont, R.; Ionov, S.; Madic, C.; Krupa, J.-C.; Guillaneux, D., A donor-acceptor model of Ln(III) complexation with terdentate nitrogen planar ligands. *New J. Chem.* **2002**, *26* (2), 234-242.
26. Guillaumont, D., Quantum chemistry study of actinide(III) and lanthanide(III) complexes with tridentate nitrogen ligands. *J. Phys. Chem. A* **2004**, *108* (33), 6893-6900.
27. Petit, L.; Adamo, C.; Maldivi, P., Toward a clear-cut vision on the origin of 2,6-di(1,2,4-triazin-3-yl)pyridine selectivity for trivalent actinides: Insights from theory. *Inorg. Chem.* **2006**, *45* (21), 8517-8522.
28. Lan, J.-H.; Shi, W.-Q.; Yuan, L.-Y.; Li, J.; Zhao, Y.-L.; Chai, Z.-F., Recent advances in computational modeling and simulations on the An(III)/Ln(III) separation process. *Coordination Chemistry Reviews* **2012**, *256* (13), 1406-1417.
29. de Sahb, C.; Watson, L. A.; Nadas, J.; Hay, B. P., Design criteria for polyazine extractants to separate An(III) from Ln(III). *Inorg. Chem.* **2013**, *52* (18), 10632-10642.
30. Zaiter, A.; Amine, B.; Bouzidi, Y.; Belkhiri, L.; Boucekkine, A.; Ephritikhine, M., Selectivity of azine ligands toward lanthanide(III)/actinide(III) differentiation: A relativistic DFT based rationalization. *Inorg. Chem.* **2014**, *53* (9), 4687-4697.
31. Yang, Y.; Liu, J.; Yang, L.; Li, K.; Zhang, H.; Luo, S.; Rao, L., Probing the difference in covalence by enthalpy measurements: a new heterocyclic N-donor ligand for actinide/lanthanide separation. *Dalton Transactions* **2015**, *44* (19), 8959-8970.
32. Fryer-Kanssen, I.; Austin, J.; Kerridge, A., Topological study of bonding in aquo and bis(triazinyl)pyridine complexes of trivalent lanthanides and actinides: Does covalency imply stability? *Inorg. Chem.* **2016**, *55* (20), 10034-10042.
33. Kovács, A.; Apostolidis, C.; Walter, O., Comparative study of complexes of rare earths and actinides with 2,6-bis(1,2,4-triazin-3-yl)pyridine. *Inorganics* **2019**, *7* (3), 26-40.

34. Lan, J. H.; Wu, Q. Y.; Wang, C. Z.; Chai, Z. F.; Shi, W. Q., Influence of complexing species on the extraction of trivalent actinides from lanthanides with CyMe₄-BTBP: A theoretical study. *J Radioanal Nucl Ch* **2018**, *318* (3), 1453-1463.
35. Bhattacharyya, A.; Ansari, S. A.; Gadly, T.; Ghosh, S. K.; Mohapatra, M.; Mohapatra, P. K., A remarkable enhancement in Am³⁺/Eu³⁺ selectivity by an ionic liquid based solvent containing bis-1,2,4-triazinyl pyridine derivatives: DFT validation of experimental results. *Dalton Transactions* **2015**, *44* (13), 6193-6201.
36. Rios, D.; Rutkowski, P. X.; Shuh, D. K.; Bray, T. H.; Gibson, J. K.; Stipdonk, M. J. V., Electron transfer dissociation of dipositive uranyl and plutonyl coordination complexes. *Journal of Mass Spectrometry* **2011**, *46* (12), 1247-1254.
37. Rios, D.; Michelini, M. C.; Lucena, A. F.; Marçalo, J.; Bray, T. H.; Gibson, J. K., Gas-phase uranyl, neptunyl, and plutonyl: Hydration and oxidation studied by experiment and theory. *Inorg. Chem.* **2012**, *51* (12), 6603-6614.
38. Lee, C.; Yang, W.; Parr, R. G., Development of the Colle-Salvetti correlation-energy formula into a functional of the electron density. *Phys. Rev. B* **1988**, *37* (2), 785-789.
39. Becke, A. D., Density-functional thermochemistry. III. The role of exact exchange. *J. Chem. Phys.* **1993**, *98* (7), 5648-5652.
40. Wu, Q.-Y.; Wang, C.-Z.; Lan, J.-H.; Xiao, C.-L.; Wang, X.-K.; Zhao, Y.-L.; Chai, Z.-F.; Shi, W.-Q., Theoretical investigation on multiple bonds in terminal actinide nitride complexes. *Inorg. Chem.* **2014**, *53* (18), 9607-9614.
41. Cao, X.; Dolg, M., Valence basis sets for relativistic energy-consistent small-core lanthanide pseudopotentials. *J. Chem. Phys.* **2001**, *115* (16), 7348-7355.
42. Cao, X.; Dolg, M., Segmented contraction scheme for small-core lanthanide pseudopotential basis sets. *Journal of Molecular Structure: THEOCHEM* **2002**, *581* (1), 139-147.
43. Francl, M. M.; Pietro, W. J.; Hehre, W. J.; Binkley, J. S.; Gordon, M. S.; DeFrees, D. J.; Pople, J. A., Self-consistent molecular orbital methods. XXIII. A polarization-type basis set for second-row elements. *J. Chem. Phys.* **1982**, *77* (7), 3654-3665.
44. Hratchian, H. P.; Schlegel, H. B., Using Hessian updating to increase the efficiency of a Hessian based predictor-corrector reaction path following method. *J. Chem. Theory Comput.* **2005**, *1* (1), 61-69.
45. Frisch, M. J.; Trucks, G. W.; Schlegel, H. B.; Scuseria, G. E.; Robb, M. A.; Cheeseman, J. R.; Scalmani, G.; Barone, V.; Petersson, G. A.; Nakatsuji, H., Gaussian 16, Revision A. 03, Gaussian. Inc., Wallingford CT **2016**.
46. Glendening, E. D.; Landis, C. R.; Weinhold, F., NBO 6.0: Natural bond orbital analysis program. *Journal of Computational Chemistry* **2013**, *34* (16), 1429-1437.
47. Shannon, R. D., Revised effective ionic radii and systematic studies of interatomic distances in halides and chalcogenides. *Acta Crystallogr A* **1976**, *32* (Sep1), 751-767.
48. Jian, T.; Dau, P. D.; Shuh, D. K.; Vasiliu, M.; Dixon, D. A.; Peterson, K. A.; Gibson, J. K., Activation of water by pentavalent actinide dioxide cations: Characteristic curium revealed by a reactivity turn after americium. *Inorg. Chem.* **2019**, *58* (20), 14005-14014.
49. Smith, P. H.; Reyes, Z. E.; Lee, C. W.; Raymond, K. N., Characterization of a series of lanthanide amine cage complexes. *Inorg. Chem.* **1988**, *27* (23), 4154-4165.
50. Caballo, J.; Garcia-Castro, M.; Martin, A.; Mena, M.; Perez-Redondo, A.; Yelamos, C., Molecular nitrides with titanium and rare-earth metals. *Inorg. Chem.* **2011**, *50* (14), 6798-6808.
51. Gong, Y.; Tian, G. X.; Rao, L. F.; Gibson, J. K., Dissociation of diglycolamide complexes of Ln(3+) (Ln = La-Lu) and An(3+) (An = Pu, Am, Cm): Redox chemistry of 4f and 5f elements in the gas phase parallels solution behavior. *Inorg. Chem.* **2014**, *53* (22), 12135-12140.

TOC Graphic

